

Corrugation of the external surface of multiwall carbon nanotubes by catalytic oxidative etching and its effect on their decoration with metal nanoparticles

M. V. Landau · S. V. Savilov · A. S. Ivanov ·
V. V. Lunin · L. Titelman · Yu. Koltypin ·
A. Gedanken

Received: 31 July 2010 / Accepted: 3 November 2010 / Published online: 17 November 2010
© Springer Science+Business Media, LLC 2010

Abstract It was established that partial combustion of carbon constituting the walls of multiwall carbon nanotubes (MWCNTs) catalyzed by previously deposited CaCO₃ nanoparticles converts parallel graphene layers in a multiwall structure to aggregates formed by nano-onions with a diameter of 5–12 nm. The areas with positive curvature of graphene layers on the external surface of air-etched MWCNTs played the role of docking stations for nickel nanoparticles inserted by sonochemical deposition after removal of the CaCO₃. The nickel nanoparticles were located exclusively at the tops of the onions. Formation of nanoscale curvature at the MWCNT support surfaces decreased the average size of Ni nanocrystals at similar loading of 50–60 wt% from 8 to 2 nm. Partial catalytic combustion did not change the concentration of surface carbonyl groups measured by titration, which attributes the observed phenomena directly to the corrugation of the MWCNT surfaces. The catalytic tests revealed a significant increase of catalytic activity of supported Ni catalyst due to corrugating of the external surface of the MWCNT support. After oxidative etching of the MWCNTs, the rate of chloroacetophenone hydrogenation measured with a

Ni–MWCNT catalyst increased by a factor of 2 without change in selectivity yielding chlorophenylethanol as the main product.

Introduction

Metal catalysts deposited on carbon nanotubes (CNTs) have been tested in many catalytic reactions demonstrating high activity and selectivity [1, 2]. The most efficient catalysts have been prepared by decoration of the external surface of mono- and multiwall-CNTs with metal nanoparticles [2, 3]. One of the important advantages of CNTs as catalysts supports is a unique opportunity to vary, on the nanoscale, the curvature of graphene sheets or of the surface formed by their edges at the exterior. The corrugation of the CNT surface strongly affects its interaction with deposited adatoms as active phases in catalytic reactions, due to tensile and compressive strains formed at the curved areas [4–6]. At the areas with positive curvature (as at the exterior CNT surface), the tensile strain increases the hybridization strength between the C-p and metal-d orbitals, facilitating the metal-support interaction and increasing the energetic barrier for metal adatom (cluster) surface diffusion [4]. This should decrease the size and increase the stability of metal nanocrystals decorating the CNT.

The noncatalytic thermal manipulations yielded ripple texturing only in single graphene layers and flat membranes with thicknesses up to 16 nm [7]. There are two options to control the curvature of the external graphene layers in CNTs at the nanoscale: to change the CNT diameter in the range of 2–10 nm, where the effect of curvature on the surface diffusion of metal adatoms is relatively strong [6], or to etch the external surface of thick multiwall CNTs (MWCNTs) with diameters of

M. V. Landau (✉) · L. Titelman
Blechner Center for Applied Catalysis and Process
Development, Department of Chemical Engineering,
Ben-Gurion University of the Negev, Beer-Sheva 84105, Israel
e-mail: mlandau@bgu.ac.il

S. V. Savilov · A. S. Ivanov · V. V. Lunin
Department of Chemistry, M. V. Lomonosov Moscow State
University, Leninskie Gory, 1-3, Moscow 119992,
Russian Federation

Yu. Koltypin · A. Gedanken
Department of Chemistry, Bar Ilan University,
Ramat Gan 52900, Israel

20–100 nm. In the last case, etching should form areas with positive curvature corresponding to a ridge-valley surface morphology with ridge heights of 2–10 nm on the external surface of the MWCNTs. The second approach looks more attractive for the preparation of metal catalysts supports since it can be applied to a wide range of relatively cheap carbonaceous materials including carbon nanofibers and in principle, allows proper control of the surface corrugation extent for any selected material.

The information collected at present about etching of CNTs shows that development of a technique for controlled corrugating of the MWCNT external surface is not a trivial problem. The chemical and electrochemical approaches using gaseous reagents or electrochemical rather than catalytic reactions in the liquid phase decreased the diameter of the MWCNTs or mostly removed tips from the CNTs external surface flattening it [8–10]. Implementation of a highly focused electron beam produced holes with negative curvature—in the walls of the MWCNT, leaving the unetched surface flat [11]. The same effect was achieved by the local steam gasification of MWCNTs after deposition of iron nanoparticles acting as a catalyst at the Fe-CNT contact interface [12]. The Fe nanoparticles penetrated deeper in the MWCNT body leaving deepening with negative curvature after their removal by acid extraction.

Recently, a successful corrugation of the external MWCNT surface was done, producing material with ridge-valley surface morphology containing ridges with positive curvature 2–7 nm in height [13]. Deposition of iron nanoparticles at this support yielded a catalyst with high stability in Fisher–Tropsch synthesis at 275 °C. The support was prepared by high-temperature pyrolysis of acetylene over iron supported on CaCO₃. The residual Ca nanoparticles remained in MWCNTs after removal of the support by HNO₃ acid extraction catalytically promoting disruption of carbon bonds in an inert atmosphere. This yielded highly localized gasification of several surface graphene layers that rendered their ridge-valley morphology. CaCO₃ is an effective catalyst of carbon combustion in air at temperatures <650 °C [14, 15]. Its deposition at the external surface of MWCNTs should provide localized carbon combustion in air that may also bring corrugation areas forming with positive curvature to the surface. This catalytic oxidation etching approach has an advantage in being applicable to any as-synthesized CNT/CNF material, independent of its synthesis history.

In the present work, it was demonstrated that the partial catalytic combustion of a MWCNT localized at the CaCO₃/CNT interface creates rolling up of graphene layers along the entire width of the MWCNT body. Conversion of the multiwall structure from parallel graphene layers to jointed onion-like aggregates produces areas with positive curvature on the external MWCNT surface. This has a strong

effect on location, dispersion, stability, and catalytic activity of Ni nanoparticles decorating the external surface of the MWCNT.

Materials and methods

Materials preparation

MWCNTs with diameters ranging from 50 to 100 nm were synthesized by direct injection of a benzene-alcohol solution of nickel acetylacetonate into a high-temperature reactor (1000 °C), followed by insertion of benzene vapor as a carbon source [16]. The residual Ni was removed by extraction with 65% HNO₃, followed by washing with THF and air drying at 80 °C. The external surfaces of parent CNTs were decorated with 15–17 nm nanoparticles of CaCO₃ (25 wt%) by carbonization of deposited Ca-nitrate implementing the CNT support as a carbon source ($\text{Ca}(\text{NO}_3)_2 + 2\text{C} \rightarrow \text{CaCO}_3 + 2\text{NO}_x + \text{CO}_y$). The deposition of Ca(NO₃)₂ salt was conducted under ultrasonication (Sonics VC750) from the saturated solution in the THF. The suspension was dried in rotavapor and the dried powder was calcined in an inert atmosphere (N₂) at 500 °C for 30 min, in order to convert the Ca(NO₃)₂ to CaCO₃.

Next, partial catalytic air-combustion of CNTs at carbon conversions of 30–50% modified the morphology of their walls. A batch of 0.4 g of CaCO₃-modified MWCNTs was placed in a tubular SS reactor with ID = 8 mm between two layers of glasswool and treated at temperatures of 450–720 °C in either a flow of He or of gas containing 5–30% O₂ (O₂-He, air), varying the flow rate and treatment time. Processes of heating to the required temperature and cooling after finishing the oxidative treatment were conducted in a flow of He. After oxidative etching, the CaCO₃ catalyst was removed from catalytically oxidatively etched CNTs (COECNT) by its treatment with HNO₃. The modified COECNT nanotubes were decorated with metallic nickel by sonochemical deposition. This was done by sonication of parent CNTs in the Ni(CO)₄ solution in decalin. The sonication (150 mg CNT in 100 mL of metal precursor solution) was conducted in a sonication flask by employing a high-intensity Ti-horn (20 kHz, 100 W/cm²) sonicator (VCX 750 Sonics & Materials) under Ar at temperatures of 5–10 °C for a period of 3 h. The metal loading was controlled by varying the concentration of a metal precursor at the sonochemical deposition step in the range of 0.02–0.5 M. After sonication, decalin was removed by decantation and the material was washed two times with pentane. These procedures were performed in a glove box (<5 ppm O₂). The resulting black powder was dried for 1 h at room temperature in a vacuum antechamber and kept inside the glove box.

Materials characterization

The prepared materials were characterized by XRD, EDAX, N₂ adsorption, Raman spectroscopy, DTG-DSC, and HRTEM methods. The metal-containing materials were protected from direct contact with air by transferring them from the glove box to measurement chambers under an inert atmosphere (HRTEM) or wetting them with decaline or isopropanol (XRD, catalytic tests).

Conventional wide-angle XRD patterns were obtained with a Philips 1050/70 powder diffractometer fitted with a graphite monochromator; software developed by Crystal Logic was used. Phase identification was performed by using a BEDE ZDS computer search/match program coupled with the ICDD (International Center for Diffraction Data) Powder Diffraction File database (2006). The crystal domain size for detected phases was determined by using the Scherrer equation $h = K\lambda/[(B2 - \beta^2)0.5 \cos(2\theta/2)]$, where $K = 1.000$ is the shape factor, $\lambda = 0.154$ nm, β is the instrumental broadening correction, and B is the experimental broadening of diffraction peaks obtained by fitting, using the Rietveld refinement. The relative content of phases represented in X-ray diffractograms was obtained by Rietveld refinement of the XRD profiles by using the DBWS-9807 program.

The metal content in Ni–CNT-supported catalysts was calculated based on metal/carbon atomic ratios, measured by energy-dispersive X-ray analysis spectroscopy (EDAX, Quanta-2000, SEM-EDAX, FEI Co) after passivation in 0.1% O₂–He flow at room temperature and by potentiometric titration of the solution, obtained after treatment of unpassivated metal-containing materials with aqueous HNO₃ (70%) in the glove box.

Surface areas, pore volumes, and pore size distributions of component powders and ground parent and coated ceramic foams were obtained from N₂ adsorption–desorption isotherms measured at 77 K in the pressure range used in conventional BET and BJH methods. The samples were outgassed under vacuum at 523 K. Isotherms were obtained at the temperature of liquid nitrogen with a NOVA-2000 (Quantachrome, version 7.11) instrument.

Differential scanning calorimetry (DSC) and gravimetric thermal analyses (TGA) were done using a TG-50-Mettler-Toledo instrument. The measurements were carried out in a flow of air or inert atmosphere (N₂) at a heating rate of 5 K min^{−1}. The Raman spectra were excited using an Ar laser ($\lambda = 488$ nm) and recorded with a Jobin–Yvon LabRaman HR 800 micro-Raman system, equipped with a liquid nitrogen cooled detector.

HRTEM analysis was conducted using a FasTEM JEOL 2010 microscope operating at 200 kV. The samples for HRTEM were prepared by depositing a drop of ethanol (MWCNT and COECNT) or pentane (metal-loaded CNT)

suspension of solid material on a carbon-coated copper grid. For Ni–CNT materials the deposition was done in the glove box, and grids were mounted at the double jilt vacuum transfer holder (model 648, Gatan Inc.) under an inert atmosphere. The holder was closed in the glove box, transferred to the microscope (JEM 2010), and connected directly to its vacuum chamber, avoiding contact of pyrophoric nickel nanocrystals with the air.

Materials performance

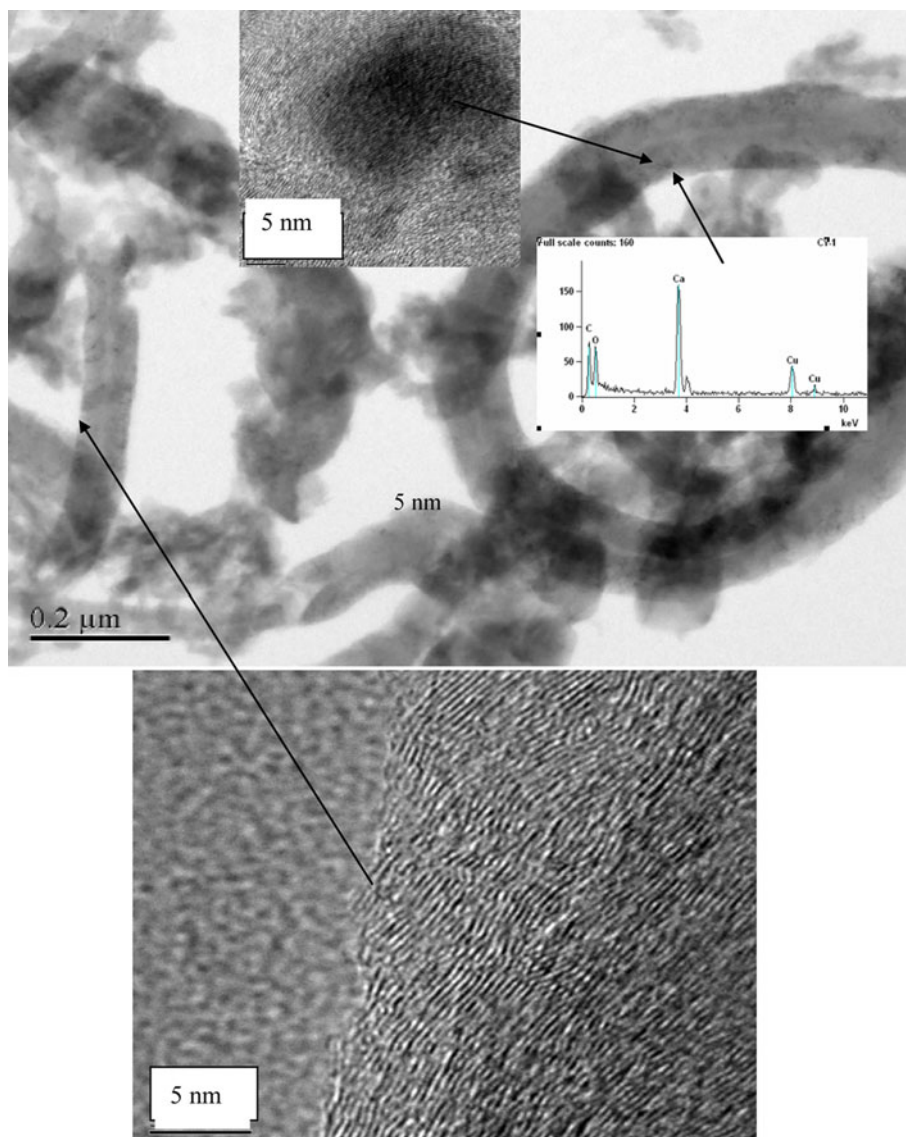
The activity and selectivity of Ni/MWCNT catalysts were tested in hydrogenation of chloroacetophenone (ClAcPh). The reaction was conducted in a stainless steel batch reactor of 20 mL volume with internal Teflon coating equipped with a magnetic mixer. The vacuum-dried catalysts were loaded in the glove box to the reactor and filled with liquid reaction mixture that protected it from air contact during the following testing steps. The testing conditions: $P_{\text{H}_2} = 30$ atm, $T = 100$ °C, catalyst loading 0.2 g, reaction mixture 0.3 g ClAcPh in 12 cm³ i-propanol, reaction time $\tau = 5$ –12 h needed for keeping the ClAcPh conversion in the range of 10–30%. The reaction rate was calculated as V [mmol/g cat.*h] = [(0.3/MW)*X]/w* τ , where X—ClAcPh conversion, MW—ClAcPh molecular weight, w—catalyst weight (gram). The contents of residual ClAcPh and its hydrogenation products were analyzed by the GC method (HP-6890 instrument equipped with FID employing a capillary DB-WAX column ($l = 30$ m, $id = 0.25$ μ m) and He as carrier gas). The 2-methoxyethyl ether was used as an internal standard. The selectivities to chlorophenylethanol (ClPhEtOH, hydrogenation route) and acetophenone (hydrodechlorination route) were calculated based on the concentrations of these compounds found in the product mixture by GC analysis.

Results and discussion

Creation of nanoscale curvature on the external surface of MWCNT by catalytic oxidative etching

The as-synthesized MWCNT had an external diameter of 50–100 nm and the diameter of the central channel was about 4–5 nm (Fig. 1). The external surface of the MWCNT was flat without nanometric indentations and close to zero curvature in the axial direction on the scale of 20–30 nm (inset in Fig. 1). The graphite layers building the MWCNT walls were nearly straight, parallel to each other, and oriented at an angle of about 45°, relative to the external surface line. At this line, they were bent forming curved external surfaces with a radial curvature diameter of 50–100 nm. The calcium-containing nanoparticles were

Fig. 1 HRTEM images of as-synthesized Ca/MWCNT material after deposition of Ca-carbonate



located on the external surface of the MWNT, visible as uniformly distributed black spots with diameters of about 15 nm (inset, Fig. 1). The local EDAX spectroscopy analysis conducted at these points, with the diameter of electron spot of 20 nm, revealed highly intensive characteristic peaks of Ca, together with carbon and oxygen (inset, Fig. 1). The Ca-containing nanoparticles were sensitive to irradiation with an electron beam during HRTEM measurements. This did not allow a clear picture of atomic layers in these nanoparticles and identification of their phase composition.

The XRD analysis, including quantitative phase analysis based on calibration curves recorded with CaCO_3 -CaO-MWCNT mechanical mixtures of different compositions, did allow identification of the nature of Ca-compounds. The XRD patterns of as-prepared Ca/MWCNT composite are shown in Fig. 2 (curve 1). Calcium existed in the

materials mostly in the form of CaCO_3 (calcite) in the amount of 29 wt% with an additional 3 wt% of CaO. Besides these and graphite phases, the samples contained residual metallic nickel (<2 wt%, 25 nm crystals), which remained after MWCNT treatment with HNO_3 before Ca deposition. The crystal domain size of CaCO_3 derived from the width of corresponding XRD peaks was 16 nm, in agreement with the HRTEM data. These data are evident for high efficiency of selected Ca-insertion methods: the Ca-nitrate deposited in the first stage was converted to nanometric CaCO_3 , as a result of decomposition and chemical interaction with the surface carbon at the second calcination stage carried out in an inert atmosphere at 500 °C.

The TGA of Ca/MWCNT material conducted in both air and N_2 atmospheres (Fig. 3a, b) displayed two peaks centered at 550 and 720°C. According to DSC data (not

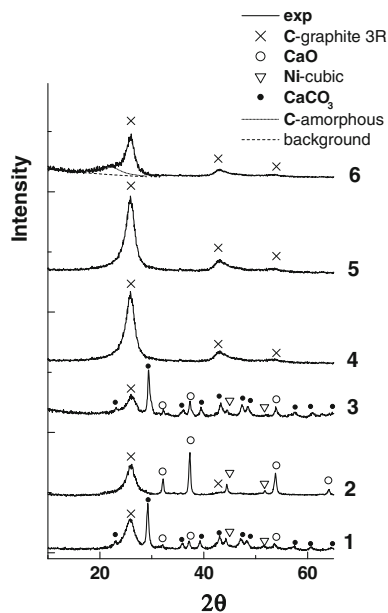


Fig. 2 XRD patterns of Ca/MWCNT material: as-synthesized (1); after treatment in He at 720 °C, 2 h (2); after treatment in He at 720 °C followed by oxidative treatment in 1 mL/min 5%O₂-He flow at 550 °C for 60 min (3); after oxidative treatment in air at 550 °C for 20 min and treatment with HNO₃ (4); after oxidative treatment in air at 550 °C for 30 min and treatment with HNO₃ (5); after oxidative treatment in air at 550 °C for 60 min and treatment with HNO₃ (6)

shown) the first was accompanied by an exothermic effect, while the second was by endothermic effect. The exothermic weight loss corresponds to the partial oxidative removal (burn-off) of carbon from the parent CNT, as a result of its catalytic oxidation to CO/CO₂. The endothermic effect reflects Ca-carbonate decomposition $\text{CaCO}_3 \rightarrow \text{CaO} + \text{CO}_2$ [14]. The ratio of integral intensities of the differential DTG peaks centered at 720/550 °C was 0.2 in air and 0.7 in nitrogen (Fig. 3, curves a, b). This reflects the relative contribution of two processes: carbon combustion ($\text{C} + \text{O}_2 \rightarrow (\text{CO})\text{CO}_2$) and Ca-carbonate decomposition, to the total sample weight loss. In nitrogen, the contribution of carbon combustion is much lower since it uses only oxygen accumulated by CaCO₃ and adsorbed by carbon. After calcination of Ca/MWCNT at 720 °C in He conducting the TGA in air significantly reduced the weight loss at 450–550 °C (Fig. 3, curve c). This corresponds to regeneration of CaCO₃, according to the reaction $\text{CaO} + \text{CO}_2 \rightarrow \text{CaCO}_3$ that occurred in this temperature range [14] and partially compensated for the weight loss caused by carbon combustion. These conclusions were confirmed by XRD data. After calcination at 720 °C in He, CaCO₃ was fully converted to CaO (Fig. 2, curve 2). After oxidative treatment at 550 °C, about 80% of the CaO phase produced during the previous step was converted back to CaCO₃ (Fig. 2, curve 3).

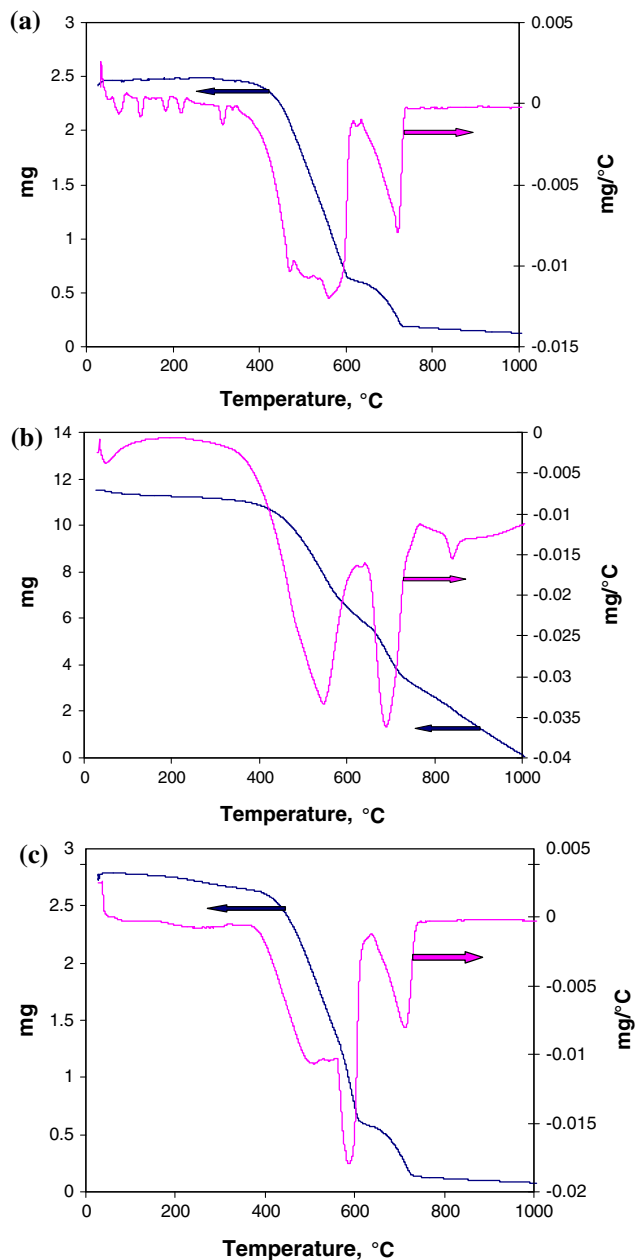


Fig. 3 TGA/DTG curves recorded with as-synthesized Ca/MWCNT material: in air (a); in N₂ (b), in air after treatment in He at 720 °C, 2 h (c)

The state of Ca-phase and oxidation conditions strongly affected the efficiency of carbon burn-off in the Ca/MWCNT material. The as-synthesized sample contained 65 wt% of the graphite phase (Table 1). The oxidative treatment of as-synthesized CaCO₃/MWCNT material containing 16 nm particles of CaCO₃ yielded relatively fast carbon burn-off. The content of the graphite phase in this material reduced by 15, 48, and 57 wt%, after treatment in air at 550 °C for 20, 30, and 60 min, respectively (Table 1, entries 6–8). Pretreatment of as-synthesized Ca/MWCNT

Table 1 Effect of oxidative treatment on the phase composition of Ca/MWCNT material

Entry	Pretreatment in He	Oxidative treatment				Phase composition		
		T (°C)	Time (min)	Treating gas		Graphite (wt%)	CaCO ₃	
				Composition	Flow (mL/min)		wt%	Crystal size (nm)
1	–	–	–	–	–	65	29	16
2	720 °C, 2 h	–	–	–	–	77	20 (CaO)	20
3	720 °C, 2 h	500	60	5%O ₂ –He	10	65	24	25
4	720 °C, 2 h	550	50	Air	25	63	26	30
5	720 °C, 2 h	550	60	Air	70	60	30	30
6	–	550	20	Air	70	50	47	20
7	–	550	30	Air	70	17	71	25
8	–	550	60	Air	70	8	82	30

material in He at 720 °C that converted CaCO₃ to CaO yielded a poor catalytic combustion effect during subsequent oxidative treatments in 5%O₂–He and in air at 550 °C at different flow rates and time periods (Table 1, entries 3–5). The content of the graphite phase was hardly decreased by 2–5 wt%. This gives direct evidence for a catalytic action of the CaCO₃ phase in graphite combustion. A similar effect of a decrease in the carbon combustion rate after calcination of CaCO₃/graphite composite in Ar and its reoxidation was observed in [17]. This was explained by decreasing the dispersion of the Ca-carbonate phase and, respectively, the interfacial contact between the catalyst particles and graphite substrate. This conclusion is in agreement with the increase of the CaCO₃ phase crystal size from 16 to 30 nm, after its conversion to CaO and regeneration back to CaCO₃ detected in the present work (Table 1). In addition, this effect of decreasing the carbon burn-off rate after decomposition-regeneration of the CaCO₃ catalytic phase can be caused only by partial regeneration of CaCO₃, while at selected temperatures only this phase displays the catalytic activity in graphite combustion. These data allow expectation of a high “selectivity” of graphite combustion—presumably at the CaCO₃/MWCNT contact interface yielding surface curvature on the scale of 10–30 nm, corresponding to the size of the CaCO₃ crystallites.

The carbon contents in oxidized Ca/MWCNT materials and their texture parameters derived from N₂ adsorption isotherms after removal of calcium are presented in Table 2. The progressive graphite combustion yielded a series of Ca/MWCNT materials where the carbon conversion changed from 17 to 95% (Table 2). Treatment of oxidized Ca/MWCNT materials with HNO₃ wholly removed the Ca-containing phases and residual nickel (Fig. 2, curves 4–6). Burning-off of 17 and 46% of the initial graphite in the Ca/MWCNT does not affect the XRD patterns of this phase, recorded after extraction of calcium (Fig. 2, curves 4, 5). It represented a layered graphite structure with layer stacking order resembling the rhombohedral 3R phase (relative integral peak intensities according to ICDD Card # 26–1079) with average inter-layer spacing of 3.4 Å. But deeper burning of the graphite body in the MWCNTs, up to 89% conversion caused formation of CaC₂ and alteration of about 30% of the graphite in remaining carbon phase to amorphous material (Fig. 2, curve 6). The latter is reflected by the appearance of the amorphous halo in XRD patterns of the oxidized material centered at 2θ = 22°. The layered graphite structure of the CNT walls survived at carbon conversion up to 50% as confirmed by Raman spectra. After extraction of residual nickel by treatment with HNO₃, the Raman spectra recorded for the parent MWCNT (not shown), contained three

Table 2 Carbon removal by selective catalytic oxidation of Ca/MWCNT and texture of air etched AEMWCNT after CaCO₃ extraction with HNO₃

Carbon content in Ca/MWCNT after air etching wt%	ΔC, gram C/100 g Ca/MWCNT	Carbon conversion (%)	Surface area (m ² /g)	Pore volume, (cm ³ /g)	Av porediameter (nm)
Not treated	–	–	216	0.41	3.8; 7–10
60	12	18	218	0.39	3.8; 6–10
50	30	46	208	0.37	3.8; 6–10
17	58	89	164	0.35	3.8; 5–10
8	62	95	–	–	–

lines: a low-frequency, weakly resolved peaks at <200 and $<500\text{ cm}^{-1}$, a large structure $\sim 1450\text{ cm}^{-1}$ (D-line), and a narrow high-frequency band between 1500 and 1700 cm^{-1} , originating from the vibrations of the $\text{C}(\text{sp}^3)$ framework (G-band). The wide low-frequency peaks do not correspond to the A_{1g} “breathing” mode in single wall carbon nanotubes. The peak width and intensities ratio of the D-line and G-band assigned to the residual ill-organized graphite and $2g$ stretching mode of well ordered graphite are characteristic for MWCNTs [18]. The catalytic oxidative etching of these MWCNTs at carbon conversion up to 46% did not significantly change the Raman spectra of the material recorded after removal of the Ca-catalyst, especially the width and D/G ratio of corresponding bands. The oxidative etching did not significantly increase the number of defects in the graphene layers. This means that the optimal conversion of graphite in air-etched Ca/AE-MWCNT materials prepared by the selective catalytic combustion route is about 50%. At such a conversion, the layered graphite structure remains undamaged, while the significant amount of removed carbon allows us to expect a major coarsening of the surface graphite layers at the nanoscale.

Burning-off a part of the carbon has no significant impact on the texture characteristics of the remaining material after Ca extraction (Table 2). At carbon conversion of 18–46%, the surface areas of residual material were in the range of 204 – $218\text{ m}^2/\text{g}$, close to its value in as-synthesized MWCNT ($216\text{ m}^2/\text{g}$). At a high carbon conversion of 89%, the surface area of residual material dropped to $164\text{ m}^2/\text{g}$. The pore volume and pore diameters

remained about the same after burning off part of the carbon.

The N_2 adsorption–desorption isotherms and pore size distributions obtained from the desorption branch of the isotherm by the BJH method are shown in Fig. 4 for parent and air-treated MWCNTs. The isotherms were recorded with the as-synthesized Ca/MWCNT after direct Ca-extraction and with the same material where Ca-extraction was done after burning off part of the carbon at a 46% carbon conversion. The peak centered at $\sim 4\text{ nm}$ can be attributed to the internal channels of MWCNTs, while pores with diameters in the range of 6 – 12 nm can be attributed to the voids between MWCNTs inside the bundles. Burning out about 50% of the carbon leaves the internal channels unharmed but slightly widens the pores inside the bundles, creating a peak centered at about 10 nm , in addition to the peak at about 7 nm that also existed before air-treatment (Fig. 4b). This may reflect the coarsening of the external surface and decreasing of the external diameter of the MWCNTs after partial carbon removal by combustion.

At a lower carbon conversion of 18%, only local morphological defects were observed in the MWCNTs by HRTEM. Increasing the carbon conversion to 46% uniformly changed the morphology of the MWCNTs along the whole CNT length. The HRTEM micrographs confirmed a decrease in the external diameter of the MWCNTs from 50 – 100 nm in the parent MWCNT (Fig. 1) to 20 – 40 nm in the AEMVCNT, with coarsening of their external surfaces at a carbon conversion of 46% (Fig. 5a). The selective catalytic combustion of carbon during this air treatment

Fig. 4 N_2 adsorption–desorption isotherms (a) and pore size distributions in MWCNT materials derived from the desorption branches of isotherms (b)

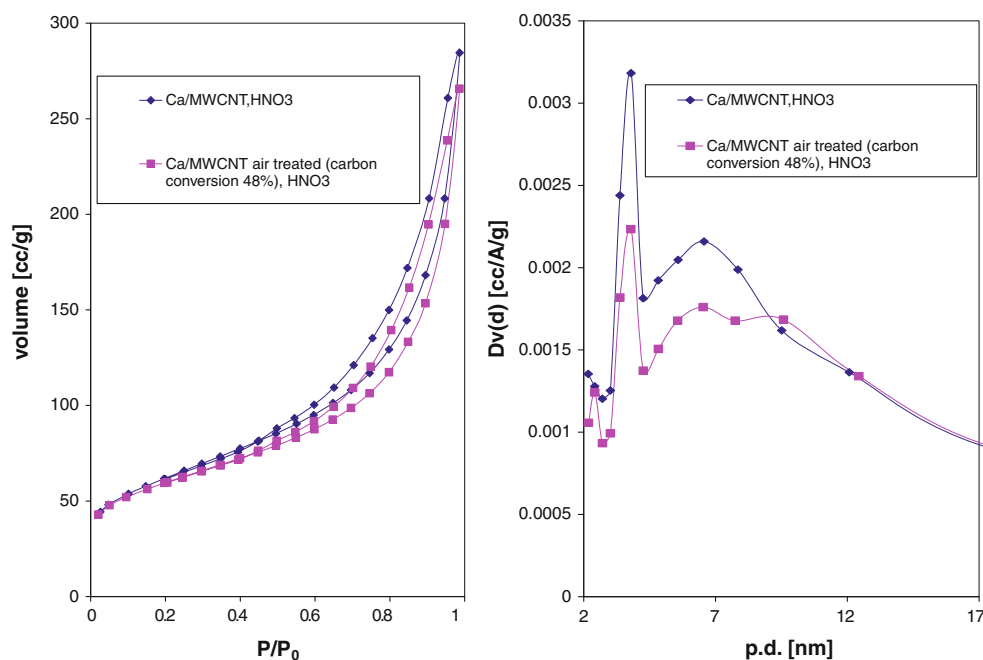
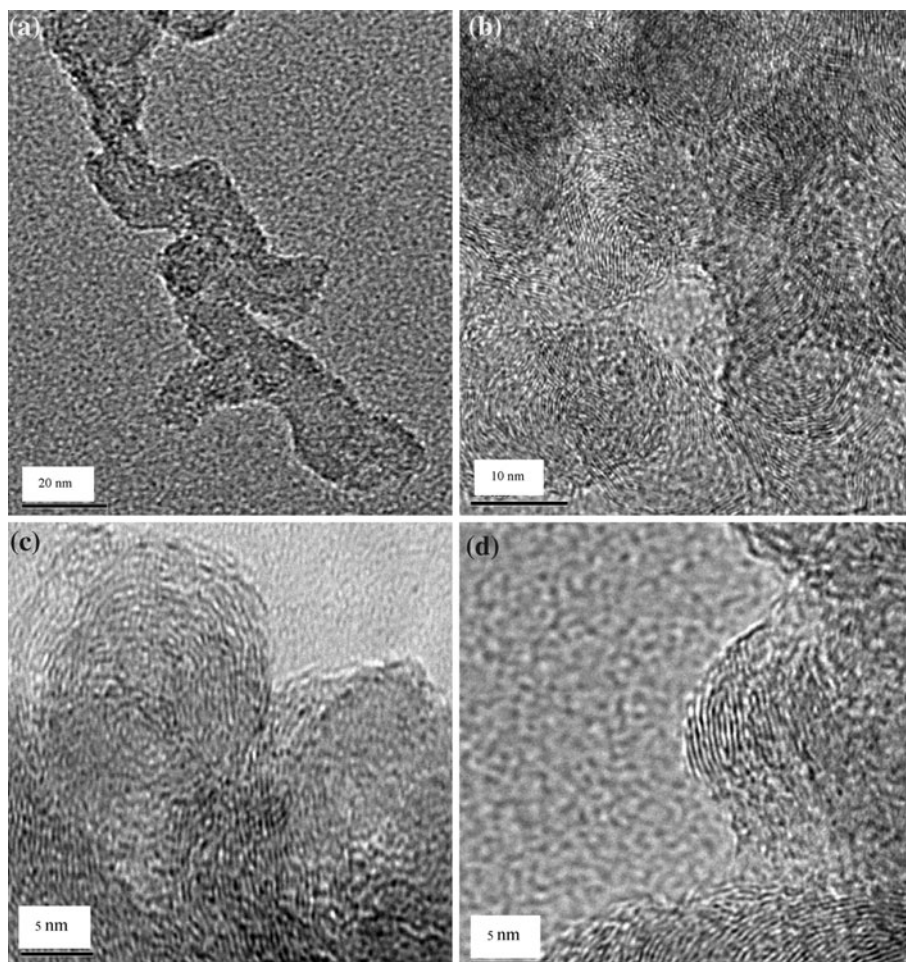


Fig. 5 TEM micrographs of AEMWCNT obtained with 46% carbon conversion at air-etching step (after calcium removal) : general view (a); nanotube wall, frontal view (b) HRTEM of nanotube external surface (side view) (c, d)



caused a drastic change in the morphology of graphene sheets in the CNT walls. The parallel graphene sheets forming the MWCNT walls were strongly curved during the air treatment, so that the structure of the AEMWCNT walls is represented by aggregates of onion-like nanometric sub-units with diameters of 5–10 nm (Fig 5b). This yielded a strong coarsening of the external surface in air treated AEMWCNTs, creating indentations of 5–15 nm in height and 15–30 nm in width, located in close vicinity in the background. The high resolution images showed that these indentations represent surface units having diameters in the range of 5–10 nm with onion structure exposing graphitic layers with positive curvature (Fig. 5c, d).

The ability to transform into units with spherical shapes is a common feature of different layered materials [19, 20]. Formation of spherical carbon nano-onions (CNOs) in a carbon material under intensive energy consumption proceeds through the appearance of graphene islands that become curved, due to the existence of defects including non-sixfold rings [21]. The CNOs appear as a result of coalescence of these curved 2D fragments, so that accumulated strain and stress yields a convex shape of the graphene layer by movement of the defects. The formation

of CNO aggregates under the catalytic oxidative etching of the MWCNTs observed in the present work can be rationalized assuming the formation of similar defective graphene fragments (islands) due to burn off of part of the graphene layers constituting the CNTs walls. This is consistent with the recent observation where only CNOs were obtained during synthesis of carbon nanotubes on a catalytic nickel substrate in the presence of oxygen [22].

Decoration of air-etched AEMWCNT with nickel nanoparticles: metal state and catalytic performance

Nickel was deposited at an AEMVCNT prepared as described above, at carbon conversion of 45–50%, after removal of residual nickel and CaCO_3 catalyst by HNO_3 extraction. 10 batches of 0.4 g $\text{CaCO}_3/\text{MWCNT}$ were treated in air at 550 °C for 20 min. The procedure was highly reproducible—the carbon conversion in these experiments varied in the range of 45–50%. The samplers were mixed together yielding 1.55 g of mixed material. The surface area of the mixed AEMWCNT material was 202 m^2/g . Its morphology, according to HRTEM analysis, was similar to that shown in Fig. 5.

Metallic nickel was deposited on this support from a nickel carbonyl solution in decalin at the conditions given above. Sonochemistry is a powerful tool for the preparation of nanoparticles of inorganic materials at mild conditions, avoiding sintering and crystal growth [23]. In the case of nickel nanoparticles, the sonochemical decomposition of the dissolved nickel carbonyl yielded metallic nickel that was directly deposited on the support mainly decorating the outer surfaces of MWCNTs with metallic nickel nanoparticles. This avoided the need for a high-temperature reduction step of deposited nickel precursor. The concentration of the nickel carbonyl in deposition solution was selected at a level that yielded 60 wt% nickel loading in the Ni/AEMWCNT catalyst according to EDAX and potentiometric titration analysis. For comparison by the same method, two reference catalysts containing 25% and 50% nickel on the parent MWCNT, treated only with HNO_3 in order to remove the residual nickel, were prepared. The XRD patterns of these three materials are presented in Fig. 6. The nickel crystal size, derived from the width of XRD reflections corresponding to the Ni° phase, increased twice (from 4 to 8 nm) after increasing of nickel loading in the parent MWCNT from 24 to 50 wt%. This is a regular behavior of the supported metallic phase: an increase in crystal size along with an increase in the metal surface concentration. By using the air-etched EAMWCNT support, it was possible to reach 60 wt% loading of metallic nickel, even decreasing the crystal size to 2 nm.

This effect could be a consequence of a strong interaction between the graphite nano-onions with positive curvature of surface grapheme layers and nickel nanoparticles, based on the theoretical considerations presented above. It was expected that nickel nanoparticles in a Ni/AEMWCNT

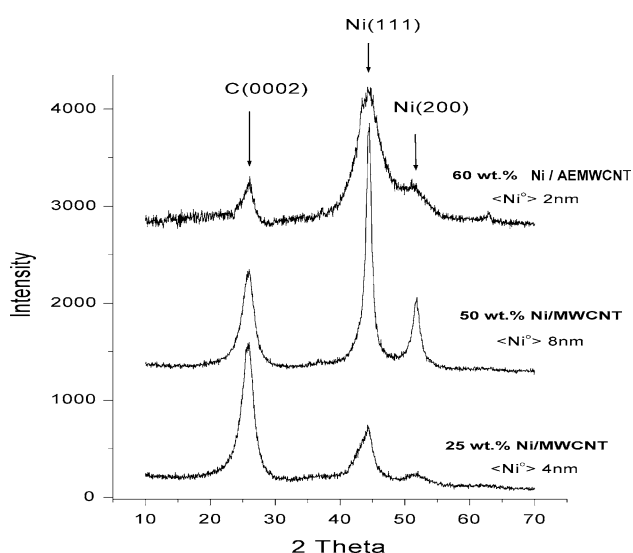


Fig. 6 XRD patterns of parent and air-etched MWCNTs decorated with nickel nanocrystals

catalyst would not be randomly distributed along all the external CNT surfaces but would be located preferably at the areas with positive nanocurvature. The comparative HRTEM analysis of reference Ni/MWCNT and Ni/AEMWCNT catalysts confirmed this expectation. The TEM images presented in Fig. 7 clearly demonstrate the difference in nickel distribution. The nanoparticles (nanoparticle aggregates) visible in low magnification TEM images appear as dark spots randomly distributed along the CNTs in the case of the reference 50 wt%Ni/MWCNT catalyst. After air-etching of the support, the Ni° phase is located at separate areas of high preference, leaving large CNT areas (shown by swords) free of nickel. The images recorded with the Ni/AEMWCNT catalyst at higher magnification (Fig. 8), showed that small (~ 2 nm) nickel nanoparticles selectively cover the areas with positive nanocurvature on the external surface of the AEMWCNTs. The graphite nano-onions exposed on the external surface of the AEMWCNTs play the role of docking stations for nickel nanoparticles, stabilizing them at high dispersion levels.

Air-etching can produce additional carboxylic groups on the external surface of MWCNTs. These groups can anchor nickel cations by ion-exchange, and even metallic nickel, as a result of electrophilic attack of their protons on valence electrons of metal atoms. This can also increase the nickel dispersion, decreasing the nickel crystal size. In order to verify this, the number of oxygen-containing surface groups in the AEMWCNT and parent MWCNT was measured by acid–base titration with NaOH, according to a procedure proposed by de Jong et al. [24], after extraction of residual nickel. The titration curves presented in Fig. 9 are evident for similar numbers of acidic surface sites (surface carboxiles). Because of the similarity of surface areas of both MWCNT materials (216 and 202 m^2/g carbon) the surface concentrations of carboxylic groups in both materials also were equal. This means that air-etching, followed by HNO_3 treatment needed for removal of the Ca-catalyst, does not increase the surface concentration of

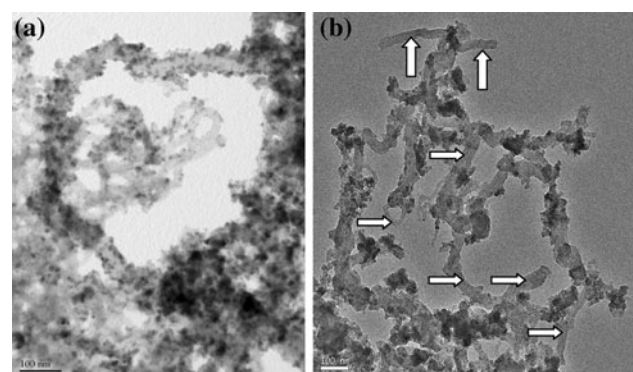


Fig. 7 Distribution of nickel nanocrystals (dark spots) at the surface of carbon nanotubes: **a** 50% Ni/MWCNT, **b** 60%Ni/AEMWCNT

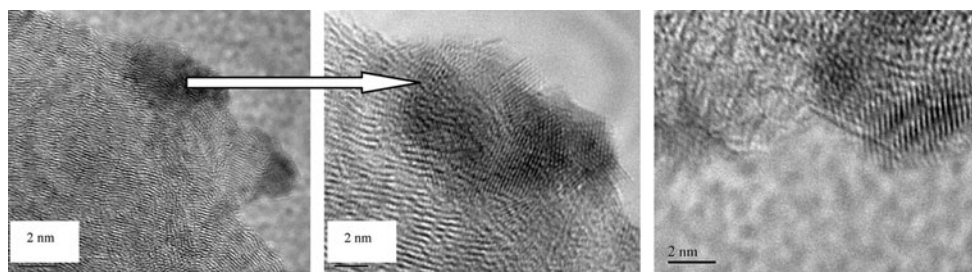


Fig. 8 HRTEM images of Ni nanocrystals in 60 wt%Ni/AEMWCNT material

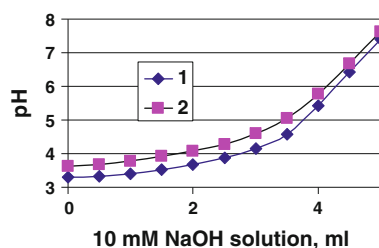


Fig. 9 Titration curves of MWCNT: 1 AEMWCNT, 2 parent MWCNT (the weight of CNT probe—40 mg)

carboxylic groups in MWCNTs relative to those formed after treatment of parent MWCNTs with HNO_3 , needed for removal of the residual nickel catalyst. Therefore, the effect of changing the distribution of nickel nanocrystals on the surface of MWCNTs observed in Fig. 7 can be fully attributed to the alteration of surface roughness—formation of areas with positive curvature on the 5–12 nm nanoscale.

The effect of air-etching of MWCNTs on the catalytic performance of the Ni–CNT catalyst was evaluated by comparative testing the activity and selectivity of reference Ni–MWCNT catalysts based on parent MWCNTs with 25 and 50 wt% metal loading and 60 wt%Ni–AEMWCNT catalyst in hydrogenation of Cl-acetophenone. Selective hydrogenation is the method of choice for reducing ketones and especially aromatic ketones as acetophenones on a large scale [25]. The advantage of Ni catalyst is their high selectivity in hydrogenation of carbonyl groups with negligible saturation of the aromatic ring. Selecting the Cl-substituted acetophenone as a substrate for catalysts testing also allowed parallel estimation of the hydrodechlorination function of prepared catalytic materials. The catalysts obtained as suspensions in decaline were washed in the glove box with isopropanol which served as a solvent for the Cl-acetophenone substrate and inserted into the reactor under liquid isopropanol avoiding air contact. Then the catalysts were tested in a batch reactor at the above listed conditions. The results are presented in Table 3. Increasing the nickel loading in reference Ni–MWCNT from 25 to 50 wt% did not significantly change the reaction rate. This can be rationalized as a result of decreasing nickel dispersion,

reflected by a decrease in the specific reaction rate normalized per gram of active metal. Insertion of even more metal (corresponding to 60 vs. 50 wt% nickel loading) to the air-etched AEMWCNTs caused about a twofold increase of catalytic activity defined as the Cl-acetophenone total conversion rate normalized per gram of catalytic material. The main reaction products were chlorophenylethanol and acetophenone, representing the two conversion routes of the substrate: hydrogenation of the carbonyl group and hydrodechlorination of the aromatic ring. Air-etching of the MWCNT support had a minor effect on the selectivity of supported nickel catalyst.

The specific reaction rate measured with 60%Ni–AEMWCNT material and normalized per gram of nickel did not grow by a factor of 2 or 4 relative to that measured with 25%Ni–MWCNT and 50%Ni–MWCNT, respectively, as could be expected based on two or four times lower nickel crystal size, taking into account the corresponding metal loadings. It seems that aggregation of nanocrystals densely covering the areas with positive curvature lowers the exposed metallic surface area compared with theoretical values expected based on the nickel crystal size. Comparison of specific reaction rates and assuming constant specific catalytic activity per 1 m^2 of Ni allows us to estimate that the effective surface area of nickel nanocrystals in 60%Ni–AEMWCNT material corresponds to the average Ni crystal size of about 5 nm rather than 2 nm, which followed from XRD/HRTEM measurements. But even in spite of partial blocking of the metallic nickel surface in aggregates, the practical effect of implementation of air-etched AEMWCNT is very significant. Using air-etched AEMWCNTs as a catalyst support compared with implementation of parent MWCNTs yielded an increase of the reaction rate measured with the same amount of catalyst of about 100% (Table 3). This reflects the strong metal-support interaction and stabilization of small nanocrystals on the curved AEMWCNTs surface at high metal loading. High stability of the metal–AEMWCNT catalysts against sintering at elevated temperatures in catalytic reactions like Fisher–Tropsch synthesis or CO_2 hydrogenation, that require higher temperatures compared with that used in the present study could also be expected.

Table 3 Testing of reference Ni/MWCNT and 60 wt%Ni/AEMWCNT catalysts in hydrogenation of chloroacetophenone (ClAcPh)

Catalytic material	Ni, wt%	Ni crystal size (XRD), nm	ClAcPh hydrogenation rate		ClAcPh hydrogenation selectivity, %	
			[mmol/g cat. * hour] × 10 ³	[mmol/g. Ni * hour] × 10 ³	CIPhEtOH	Acetophenone
Ni/MWCNT	25	4	228	912	67.2	15.6
Ni/MWCNT	50	8	234	468	69.2	21.0
Ni/AEMWCNT	60	2	463	771	64.2	26.3

Testing conditions: batch reactor; $T = 100\text{ }^{\circ}\text{C}$, $P_{\text{H}_2} = 30\text{ atm}$, starting reaction mixture: 0.3 g ClAcPh in 12 mL of i-PrOH

Conclusions

The selective catalytic combustion of carbon in MWCNTs at the contact interface with 15–17 nm particles of a CaCO_3 catalyst caused coarsening of graphitic layers due to formation of carbon nano-onions. This yielded indentations with 5–12 nm positive curvature diameters at the surface of the MWCNTs after burning off 45–50% of the carbon that converted the structure of the MWCNTs multilayered graphite walls to aggregates of graphite onions 5–12 nm in size. This created high surface concentration of “docking stations” for nanoparticles of the guest catalytic nickel phase. Stabilizing of aggregates of 2 nm nickel nanocrystals at the surface of air-etched AEMWCNTs at high nickel loading (60 wt%) allowed an increase in the catalytic activity of Ni–MWCNT material prepared by ultrasonical deposition by a factor of about 2.

Acknowledgements This study was supported by a joint MSTI-RFBR program: Grants #3-3549 and # 3-5739 (Israel Ministry of Science and Technology) and Grants # 09-03-92482 and 06-03-72032 (Russian Foundation for Basic Research). The authors gratefully acknowledge the help of Dr. A.Erenburg (XRD), Dr. V. Ezersky (HRTEM), and Dr. J. Grinblat (HRTEM) for conducting the materials characterizations.

References

- Serp P, Corrias M, Kalck K (2003) *Appl Catal A* 253:337
- Georgakilas V, Cournis D, Tzitzios V, Pasquato L, Guldi DM, Prato M (2007) *J Mater Chem* 17:2679
- Wildgoose GG, Banks E, Compton RG (2006) *Small* 2:182
- Menon M, Andriotis AN, Froudakis GE (2000) *Chem Phys Lett* 320:425
- Shu DJ, Gong XJ (2001) *J Chem Phys* 114:10922
- Wu M-C, Li C-L, Hu C-K, Chang Y-C, Liaw Y-H, Huang L-W, Chang C-S, Tsong T-T, Hsu T (2006) *Phys Rev B* 74:125424/1
- Bao W, Miao F, Chen Z, Zhang H, Jang W, Dames C, Lau CN (2009) *Nat Nanotechnol* 4:562
- Yu G, Gong J, Wang S, Zhu D, He S, Zhu Z (2006) *Carbon* 44:1218
- Ye J-S, Mo J, Zhang WD, Liu X, Sheu F-S (2008) *NANO* 3:461
- Ito T, Sun L, Crooks RM (2003) *Electrochem Solid State Lett* 6:C4
- Aref T, Remeika M, Bezryadin A (2008) *J Appl Phys* 104:024312/1
- Xia W, Hagen V, Kundu S, Wang Y, Somsen C, Eggler G, Sun G, Grundmeier G, Stratmann M, Muhler M (2007) *Adv Mater* 19:3468
- Graham UM, Dozier A, Khatri RA, Bahome MC, Jewell LL, Mhlanga SD, Coville NJ, Davis BH (2009) *Catal Lett* 129:39
- Levendis YA, Nam SW, Lowenberg M, Flagan RC, Gavalas GR (1989) *Energy Fuels* 3:28
- Tomita A (2001) *Catal Surv Jpn* 5:17
- Savilov SV, Zosimov GA, Lunin VV (2007) *Russ. Patent RU* 2310601
- Wu X, Radovic LR (2005) *Carbon* 43:333
- Belin T, Epron F (2005) *Mater Sci Eng B* 119:105
- Tenne R, Margulis L, Genut M, Hodes J (1992) *Nature* 360:444
- Saito Y, Yoshikawa T, Inagaki M, Tomita M, Hayashi T (1993) *Chem Phys Lett* 204:277
- Szerencsi M, Radnoczi G (2010) *Vacuum* 84:197
- Hou S-S, Chung D-H, Lin T-H (2009) *Carbon* 47:938
- Gedanken A, Koltypin Y, Perkas N, Besson M, Vradman L, Herskowitz M, Landau MV (2004) *Trans Indian Ceram Soc* 63:137
- Toebes ML, van Heeswijk UJMP, Bitter JH, van Dillen AJ, de Jong KP (2004) *Carbon* 42:307
- Blaser H-U, Malan C, Pugin B, Spindler F, Steiner H, Studer M (2003) *Adv Synth Catal* 345:103